

Optical properties of surface-tunable NiO films depending on oxygen pressure, growth temperature, and growth duration

Sung Lim Ko^a, Youngwook Noh^b, Chang-Wan Kim^a, Dongjin Lee^{a,c}, Chongmu Lee^d and Changhyun Jin^{a,*}

^aSchool of Mechanical Engineering, Konkuk University, Seoul 143-701, Korea

^bDepartment of Mechanical Design and Production Engineering, Konkuk University, Seoul 143-701, Korea

^cFlexible Display Roll-to-Roll Research Center, Konkuk University, Seoul 143-701, Korea

^dDepartment of Materials Science and Engineering, Inha University, 253 Yonghyun-dong, Nam-gu, Incheon 402-751, Korea

Nanostructures based on thin oxide films have a number of applications. In this work, we report the physical and optical properties of a wide range of NiO thin film nanostructures. These films were fabricated using thermal oxidation of a Ni substrate with different oxygen partial pressures, growth temperatures, and growth durations. SEM observations of NiO films evaporated in static air to 200 sccm O₂ partial pressure conditions show the evolution of the microstructure from initially coarse islands or particles to well-formed NiO thin films combined with neighboring structures. The root-mean-square crystallite sizes from AFM measurements were 50.769 nm and 137.66 nm for temperatures of 620 °C and 730 °C and durations of 4 and 6 h, respectively. X-ray diffraction was performed to understand the microstructure of the two-dimensional NiO thin films in more detail. Photoluminescence (PL) spectra of the NiO films reveal that the both the PL intensity and energy vary with respect to oxygen pressure, temperature, and duration. The mechanisms for the different observed microstructures and the optical transitions in the NiO thin films are considered.

Key words: semiconducting oxide, thin films, microscopy, photoluminescence.

Introduction

There has been considerable attention aimed at developing low-dimensional (0D, 1D, and 2D) nanomaterials, especially transitional metal oxides, owing to their remarkable physical and chemical properties in various practical applications and fundamental research. Transition metal oxide nanomaterials are of interest in the optical [1], electrical [2], electrochemical [3], catalytic [4], optoelectronic [5], electronic [6], and magnetic [7] fields. Among the low-dimensional metal oxides, NiO-based nanostructures are of particular interest, for example, as NiO (1) is a p-type semiconductor with a wide band gap (3.5 eV–4.0 eV) [8], (2) has a high sensitivity to nickel defects [9], (3) has an improved lithium storage ability [10], and (4) is a matrix for the immobilization of biomolecules [11]. Many kinds of synthesis methods have been investigated for NiO-based nanomaterials. Some of these methods include hydrothermal reaction [12], flame-fusion (Verneuil) [13], electron beam evaporation [14], microwave or conventional combustion methods [15], sonochemical methods [16], and DC reactive magnetron sputtering [17]. These synthesis methods can be used to produce controlled microstructures and elemental compositions, such as flower or sea urchin-like hierarchical

nanostructures [18, 19], hollow microspheres [20], concave polyhedrons [21], nanoplates [22], and nanosheets [23]. As nanoscale devices have received much attention, 2D nanostructures are becoming more important owing to their exceptionally large surface area. In this work, NiO thin films were synthesized using thermal oxidation under different oxygen partial pressures, temperatures, and durations, and their optical properties and microstructures were examined as a function of these process variables.

Experimental

A Ni substrate cut into dimensions of 2 × 2 cm² was placed on a crucible boat. The boat was then positioned at the center of a horizontal tube furnace. The furnace was then heated to different temperatures at a rate of 60 °C/min. The oxidation temperature, oxygen partial pressure, and time were varied. The process variables for the different NiO nanostructures formed using thermal oxidation are summarized here. (1) To understand the effect of oxygen pressure, different gas flow rates were used during synthesis, including a constant 300 sccm N₂ gas flow and O₂ gas flow rates of 0, 50, 100, 150, and 200 sccm at 620 °C for 4 h. A flow rate of 0 sccm corresponds to static air in the tube furnace. (2) To understand the effect of temperature, oxidation was performed at two different temperatures of 620 °C and 730 °C at a constant 200 sccm O₂ gas flow. (3) The effect of time was studied by annealing

*Corresponding author:
Tel : +82-2-450-3482
Fax: +82-2-447-5886
E-mail: jinch@konkuk.ac.kr

under the same conditions described in (2) for two different hold times of 4 h and 6 h. All the samples were cooled to room temperature in the tube furnace.

The morphologies of the final NiO thin film products were investigated by scanning electron microscopy (SEM, Hitachi S-4200) and atomic force microscopy (AFM, Multimode Iva). The microstructural and compositional analysis of the individual products were performed using X-ray diffraction (XRD) with a glancing angle of 0.5° (X'pert MPD, Philips, with $\text{Cu-K}\alpha$ radiation). In addition, for studying the optical properties of 2D NiO samples, photoluminescence (PL) measurements (SPEC-1403 PL spectrometer (Kimon, 1K, Japan)) were taken at room temperature from a 325 nm He-Cd laser source.

Results and Discussion

Fig. 1 shows oxygen-dependent SEM images of NiO thin films synthesized at 620°C for 4 h via thermal oxidation of a Ni substrate. With an increase of oxygen partial pressure, the NiO nanoparticle sizes seem to gradually decrease up to 100 sccm O_2 gas. Above this flow rate, new aggregation or growth of NiO nanostructures occurs. Most of the NiO nanostructures shown in Fig. 1(a), below 100 sccm, consist of big aggregates, arising from heterogeneous nucleation. At a higher concentration of oxygen (Fig. 1(b,c)), further condensation of Ni or NiO seeds occurs easily on the Ni substrate. These seeds then act as new nucleation sites or contribute to the growth of preformed nucleation sites, exhausting additional O atoms. Most importantly, all homogeneous seeds for NiO nucleation occur over the entire surface area simultaneously for flow rates of under 100 sccm O_2 , as seen in Fig 1(c). Higher O_2 flow rates, for example, for both 150 sccm and 200 sccm pressure conditions (Fig. 1(d,e)), contribute to fast nucleation kinetics, implying the formation of extra nucleation sites, rather than the growth of preformed NiO nanostructures

caused by an improved diffusion rate. Therefore, O_2 gas flow rates above 100 sccm do not seem to be sufficient for the growth of NiO, but rather generate much finer nucleation sites for the formation of NiO, as shown in Fig. 1(f).

Four different SEM images for samples synthesized with different temperatures and times are shown in Fig. 2. At 620 °C for 4 h with a 200 sccm O_2 flow rate (Fig. 2(a)), many nanoclusters form on the surface of the Ni substrate. The sizes of nanoclusters are approximately a few tens of nanometers. When the durations are 2 h longer than those of Fig. 2(a) under the same temperature and flow rate conditions, the existing nanoclusters begin to aggregate with adjacent nanoclusters, yielding new, larger nanoclusters about 100 nm-300 nm in size (Fig. 2(b)) in order to decrease their surface energy. For NiO films formed at a higher temperature of 730 °C, a duration of 4 h, and 200 sccm O_2 , as shown in Fig. 2(c), larger, island-like structures continuously combine with the neighboring island-like structures. These structures tended to aggregate,

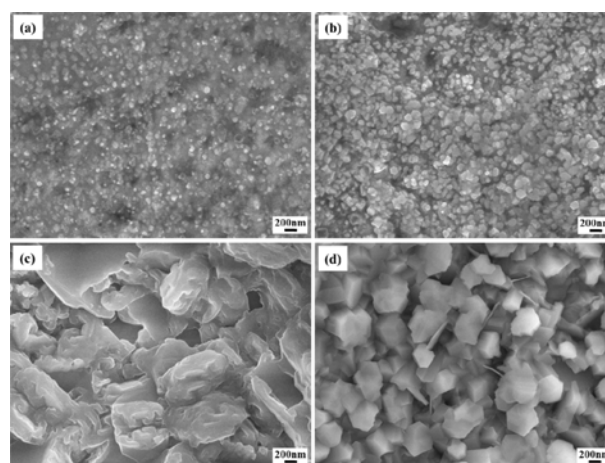


Fig. 2. SEM images of NiO nanostructures synthesized under different temperatures and durations with a fixed flow rate of 200 sccm O_2 . (a) 620 °C for 4 h (b) 620 °C for 6 h (c) 730 °C for 4 h (d) 730 °C for 4 h.

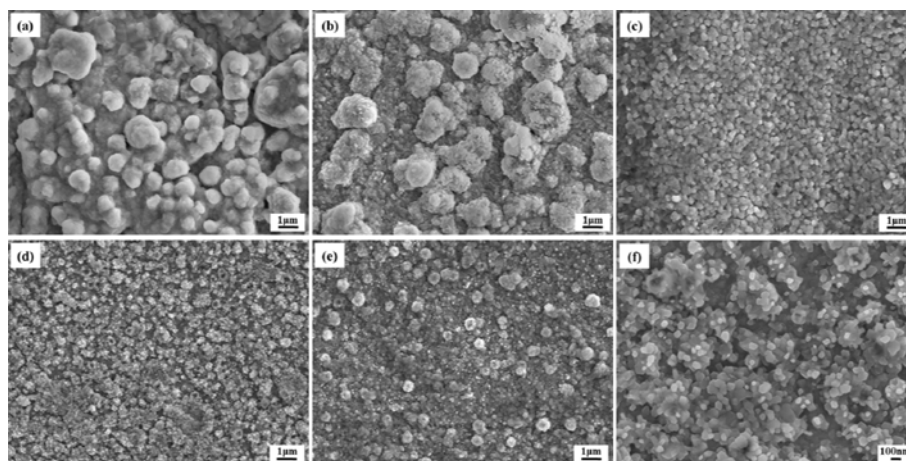


Fig. 1. SEM images of a NiO nanostructure synthesized at 620 °C for 4 h with (a) static air, (b) 50 sccm O_2 , (c) 100 sccm O_2 , (d) 150 sccm O_2 , and (e,f) 200 sccm O_2 .

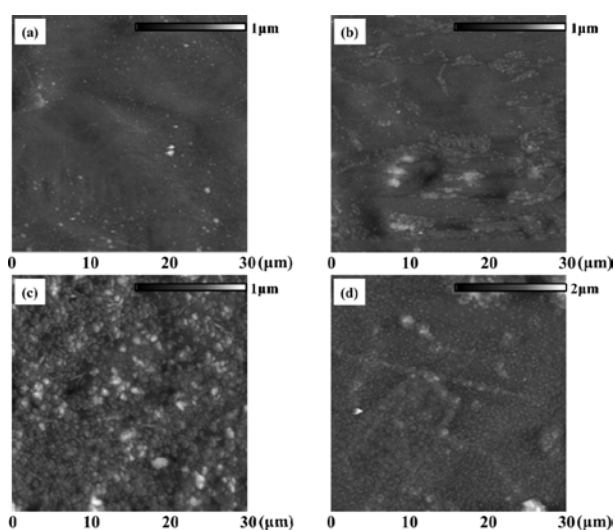


Fig. 3. Surface morphologies of NiO thin films for different temperatures and durations at a fixed flow rate of 200 sccm O_2 . (a) 620 °C for 4 h (b) 620 °C for 6 h (c) 730 °C for 4 h (d) 730 °C for 6 h.

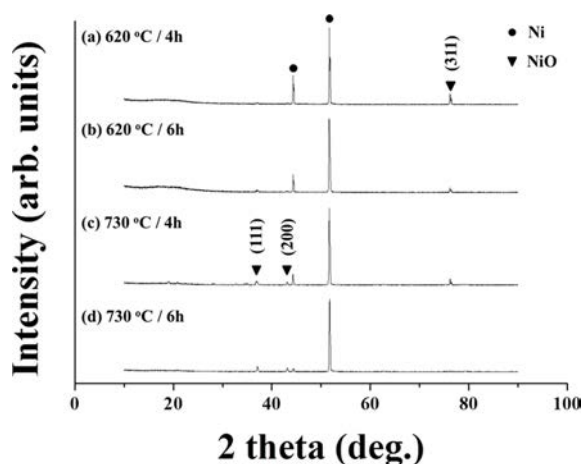


Fig. 4. XRD patterns of NiO thin films related to different temperature and durations.

forming a sparser and thicker surface on the NiO nanostructures. When the NiO thin films are synthesized under the same conditions as in Fig. 2(c), but for 6 h instead of 4 h, high density NiO nanomasses and low-density NiO nanowalls are found. This result means that the extra energy arising from the 2 h longer process times is sufficient for the formation of partly faceted nanoparticles and thin nanowalls.

AFM was used to investigate the surface morphology of NiO thin films synthesized at 620 °C and 730 °C. Fig. 3(a) shows a NiO film synthesized at 620 °C for 4 h with a 200 sccm O_2 flow rate. This sample has uniform grains with a root-mean-square (RMS) crystallite size of 50 nm. On the other hand, with increasing times (Fig. 3(b)) and temperatures (Fig. 3(c)), the probability of hills and the sharpness of hills increases in the Ni thin films. At the highest temperature and longest duration condition studied here in Fig. 3(d), the crystallite size was approximately 137 nm RMS. This result is contrary to the SEM images

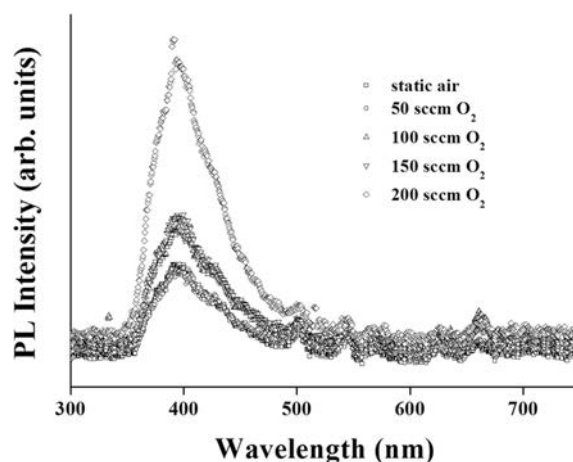


Fig. 5. Room temperature PL spectra of NiO nanostructures synthesized with different O_2 flow rates.

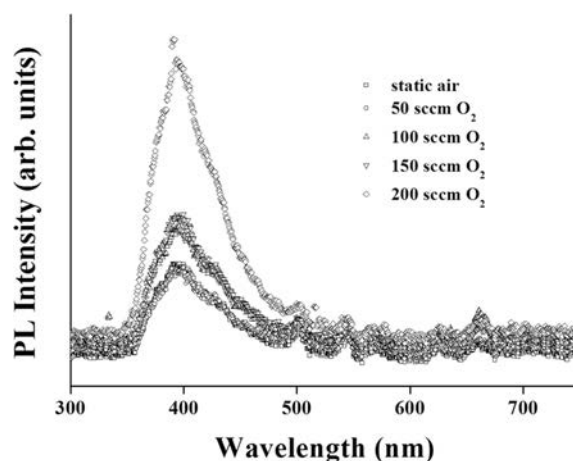


Fig. 6. Room temperature PL spectra of NiO nanostructures synthesized under different temperatures and durations.

shown in Fig. 2(d). We conclude that higher temperature and longer duration during NiO thin film formation assist the formation of new nucleates, such as mixed nanomasses and nanowalls or grain growth of preformed NiO crystallites simultaneously.

Fig. 4 shows the XRD patterns of NiO thin films for different process variables. The XRD patterns of NiO (Fig. 4(a)) for a temperature of 620 °C and a duration of 4 h revealed the main diffraction peaks of the Ni substrate and the (311) peak of the NiO thin film. No NiO nanocrystalline peaks were observed for 620 °C and 6 h conditions, as shown Fig. 4(b). However, XRD patterns at 730 °C (Fig. 4(c,d)) showed strong NiO peaks at the (111), (200), and (311) positions, implying that these peaks are well matched with cubic NiO crystals (JCPDS card No. 89-7130). In particular, the intensity of the Ni substrate peaks rapidly decreases with increasing temperature and duration. We believe that elevated temperature can induce a higher diffusion rate of the Ni^{2+} ions, increasing the possibility that Ni^{2+} ions move to the surface of the Ni substrate, react with oxygen, and form NiO nanostructures on the surface.

From previous reports [24, 25], the PL from NiO nanostructures in the UV region are associated with a recombination of excitons, affected by the stoichiometric arrangement of cations and anions [24]. Therefore, both PL intensity and wavelength in the UV region for NiO nanostructures are influenced by the purity and crystallinity. The PL spectra of NiO nanostructures are also affected by defects resulting from the non-stoichiometric alignment of microstructures [25]. Hence, both PL intensity and energy at defects in the NiO nanostructures are controlled by impurities in NiO samples.

Fig. 5 displays the PL spectra for five different O₂ conditions in NiO thin films. The PL spectrum without O₂ gas shows one strong UV emission peak and some weak emission peaks related to the degree of defect levels. Progressively increasing the oxygen partial pressure from 50 sccm to 200 sccm results in PL spectra with a strong UV band near 390 nm–400 nm. This trend implies that the O₂ pressure can improve the crystallinity and stoichiometry of NiO thin films.

Fig. 6 shows the change of PL spectra for different temperatures and durations. First, the PL spectrum at 620 °C with a flow rate of 200 sccm for 4 h, shows a UV emission peak around 395 nm and orange and red emission peaks near 660 nm and 680 nm, respectively. The defect level emission peaks occasionally disappear, as seen in Fig. 5. Second, when NiO thin films are synthesized for 2 h longer, the PL spectrum is largely the same as in the previous condition. Third, under a higher synthesis temperature at 730 °C for 4 h, the UV PL intensity increases somewhat at 395 nm and some defect level emission peaks appear at 500 nm, 545 nm, and 570 nm. Finally, the PL properties for 6 h at a temperature of 730 °C exhibit a strong UV emission band and some weak defect level bands depending on the recombination density and the different types of defects in the NiO thin films. These features arise from homogeneous nucleation and the generation of new defects on NiO substrates for longer durations. This finding is confirmed by previous reports. For example, Mohammadyani *et al.* [16] have suggested that the UV emission can be attributed to direct exciton–exciton scattering. Malandrino *et al.* [26] have reported that the dangling bonds on NiO nanotube walls cause defect densities localized in the gap arising from a decrease in fundamental absorption. Founded on different PL properties, we deduce that various process variables enable the PL spectra in NiO thin films to have different numbers and types of recombination behavior and defects depending on the microstructure.

Conclusions

Several NiO thin films were synthesized by thermal oxidation of a Ni substrate under various process variable conditions: (1) different O₂ partial pressures from static air to 200 sccm O₂ flow rates, (2) oxidation

temperatures of 620 °C and 730 °C, and (3) oxidation times of 4 h and 6 h. SEM and AFM images of the different NiO thin films show gradual distinct morphologies representing the distinct nucleation and growth processes of NiO. XRD analysis indicates that NiO thin films consist of cubic NiO crystals regardless of their synthesis condition. The degree of crystallinity and the preferred orientation change with synthesis conditions. The PL properties of NiO nanostructures are related to the presence or absence of exciton recombination and the quantity of defects during the thermal oxidation process. Therefore, optical applications based on NiO thin films can be tailored by suitably controlling the O₂ gas flow, oxidation temperature, and oxidation duration.

Acknowledgments

This paper was supported by the KU Research Professor Program of Konkuk University. And this research was supported by Basic Science Research Program through the National Research Foundation of Korea(NRF) funded by the Ministry of Education (NRF-2010-00525).

References

1. F. Flory, L. Escoubas, G. Berginc, *J. Nanophoton* 5 (2011) 052502.
2. M.G. Deceglie, V.E. Ferry, A.P. Alivisatos, H.A. Atwater, *Nano Lett.* 12 (2012) 2894–2900.
3. G. Yu, X. Xie, L. Pan, Z. Bao, Y. Cui, *Nano Energy* 2 (2013) 213–234.
4. G.R. Zhang, D. Zhao, Y.Y. Feng, B. Zhang, D.S. Su, G. Liu, B.Q. Xu, *ACS Nano* 6 (2012) 2226–2236.
5. H. Li, X. Wang, J. Xu, Q. Zhang, Y. Bando, D. Golberg, Y. Ma, T. Zhai, *Adv. Mater.* 25 (2013) 3017–3037.
6. J.Q. He, J.R. Sootsman, L.Q. Xu, S.N. Girard, J.C. Zheng, M.G. Kanatzidis, V.P. Dravid, *J. Am. Chem. Soc.* 133 (2011), 8736–8789.
7. H. Yamane, K. Takeda, M. Kobayashi, *Appl. Phys. Lett.* 106 (2015) 052409.
8. J.D. Desai, S.K. Min, K.D. Jung, O.S. Joo, *Appl. Surf. Sci.* 253 (2006) 1781–1786.
9. B. Subramanian, M.M. Ibrahim, K.R. Murali, V.S. Vidhya, C. Sanjeeviraja, M. Jayachandran, *J. Mater. Sci.* 20 (2009) 953–957.
10. Y. Li, B. Tan, Y. Wu, *Chem. Mater.* 20 (2008) 567–576.
11. C. Li, Y. Liu, L. Li, Z. Du, S. Xu, M. Zhang, X. Yin, T. Wang, *Talanta* 77 (2008) 455–459.
12. B. Liu, H. Yang, H. Zhao, L. An, L. Zhang, R. Shi, L. Wang, L. Bao, Y. Chen, *Sens. Actuators B* 156 (2011) 251–262.
13. S. Mochizuki, T. Saito, *Physica B* 404 (2009) 4850–4853.
14. D.Y. Jiang, J.M. Qin, X. Wang, S. Gao, Q.C. Liang, J.X. Zhao, *Vacuum* 86 (2012) 1083–1086.
15. A. Manikandan, J.J. Vijaya, L.J. Kennedy, *Physica E* 49 (2013) 117–123.
16. S.M. Meybodi, S.A. Hosseini, M. Rezaee, S.K. Sadrnehaad, D. Mohammadyani, *Ultrason. Sonochem.* 19 (2012) 841–845.
17. B. Subramanian, M.M. Ibrahim, V. Senthilkumar, K.R. Murali, V.S. Vidhya, C. Sanjeeviraja, M. Jayachandran,

- Physica B 403 (2008) 4104-4110.
18. X. Ni, Y. Zhang, D. Tian, H. Zheng, X. Wang, *J. Cryst. Growth* 306 (2007) 418-421.
 19. L. Bai, F. Yuan, P. Hu, S. Yan, X. Wang, *Mater. Lett.* 61 (2007) 1698-1700.
 20. D. Wang, C. Song, Z. Hu, X. Fu, *J. Phys. Chem. B* 109 (2005) 1125-1129.
 21. X. Wang, L. Yu, P. Hu, F. Yuan, *Cryst. Growth Des.* 7 (2007) 2415-2418.
 22. X. Wang, L. Li, Y. Zhang, S. Wang, Z. Zhang, L. Fei, Y. Qian, *Cryst. Growth Des.* 6 (2006) 2163-2165.
 23. J.Y. Zhang, H.Q. Yang, Y.Z. Song, D.C. Chen, L. Li, H. Jiao, *Acta Chime. Sinica (in Chinese)* 65 (2007) 2069-2075.
 24. K. Anandan, V. Rajendran, *Mat. Sci. Semicon. Proc.* 14 (2011) 43-47.
 25. S. Mochizuki, T. Saito, *Physica B* 404 (2009) 4850-4853.
 26. G. Malandrino, L.M.S. Perdicaro, I.L. Fragala, R.L. Nigro, M. Losurdo, G. Bruno, *J. Phys. Chem. C* 111 (2007) 3211-3215.